Does Photomineralization of Dissolved Organics Matter in Temperate Rivers?

Taylor Maavara[1] , Laura Logozzo[1] , Aron Stubbins[2] , Kelly Aho[1] ,
Craig Brinkerhoff[3] , Jacob Hosen[4] , and Peter Raymond[1]

[1]School of the Environment, Yale University, New Haven, CT, USA, [2]Department of Marine and Environmental Sciences, Civil and Environmental Engineering, and Chemistry and Chemical Biology, Northeastern University, Boston, MA, USA, [3]Department of Civil and Environmental Engineering, University of Massachusetts, Amherst, MA, USA, [4]Department of Forestry and Natural Resources, Purdue University, West Lafayette, IN, USA

Abstract Sunlight can oxidize dissolved organic carbon (DOC) to dissolved inorganic carbon (DIC) in freshwaters. The importance of complete photooxidation, or photomineralization, as a sink for DOC remains unclear in temperate rivers, as most estimates are restricted to lakes, high latitude rivers, and coastal river plumes. In this study, we construct a model representing over 75,000 river reaches in the Connecticut River Watershed (CRW), USA, to calculate spectrally resolved photomineralization. We test the hypothesis that photomineralization is a negligible DOC sink across all reaches and flow conditions relative to DOC fluxes. Our model quantifies reaction rates and transport drivers within the river reaches for the ranges of flow conditions, incoming solar irradiance, and canopy cover shading observed throughout the year. Our model predicts average daily areal photomineralization rates ranging from 1.16 mg-C m^{-2} day^{-1} in low flow river reaches in the winter, to 18.33 mg-C m^{-2} day^{-1} in high flow river reaches during the summer. Even for high photomineralization fluxes, corresponding photomineralization uptake velocities are typically at least an order of magnitude smaller than those reported for other instream processes. We calculate DOC elimination by photomineralization relative to DOC fluxes through individual stream reaches as well as the entire riverine portion of the CRW. We find that relative photomineralization fluxes are highest in summer drought conditions in low order streams. In median flows and mean light intensities, for an average watershed travel distance, 3%–5% of the DOC fluxes are eliminated, indicating that photomineralization is a minor DOC sink in temperate rivers.

Plain Language Summary Rivers are an important part of the carbon cycle, moving carbon compounds from land to the ocean. Within rivers, dissolved organic carbon molecules can be broken down into inorganic carbon molecules, including the greenhouse gas carbon dioxide. Sunlight shining into rivers can cause these organic molecules to break down in a process called photomineralization, but it is not clear if this process is important compared to the total amount of organic carbon that travels through rivers every day. In this paper, we build a model for the river sections of temperate Connecticut River Watershed, which calculates photomineralization for possible river flow conditions, dissolved organic carbon concentrations, and seasons, and compares the size of the sunlight-driven breakdown of dissolved organic carbon to the amount of dissolved organic carbon in the river. This is the first model that puts photomineralization rates in the context of a flowing temperate river network. We show that compared with the dissolved organic carbon amounts present in the river at any time of the year or any flow conditions, photomineralization is essentially an unimportant process, removing on average 3%–5% of the dissolved organic carbon through an average watershed river route.

1. Introduction

Dissolved organic matter (DOM) is one of the largest fluxes of carbon in inland water ecosystems and a central component of riverine metabolism. DOM, which is approximately 50% dissolved organic carbon (DOC) by mass (Dittmar & Stubbins, 2014; Krogh, 1934), is a nutrient and energy source, capable of transporting metals and pollutants, and a driver of light availability in water bodies (Kaplan & Cory, 2016; Schlesinger & Melack, 1981). Large amounts of riverine DOC enter the ocean annually, where it is an important source of reduced carbon (Raymond & Spencer, 2015). Although the amount of DOC entering the ocean is relatively well known, its representative chemical composition, reactivity, and the seasonality of its input are not as

well established. This is in part due to a lack of an estimate of the amount of terrestrial DOC entering rivers, of autochthonous DOC added to drainage networks, and of the proportion of DOC removed by in-situ processes such as microbial uptake and photooxidation. Regional-to global-scale estimates of these processes are hampered by high temporal variability driven by hydrology and heterogenic terrestrial landscapes, and until recently, a lack of a representation of drainage networks for modeling. Key uncertainties remain regarding DOC transformation pathways to dissolved inorganic C (DIC), including carbon dioxide (CO_2) (Battin et al., 2009; Cole et al., 2007; Raymond et al., 2013). Photochemical oxidation, or photooxidation, is one pathway that can drive the alteration or transformation of DOC molecules in freshwater bodies, as colored or chromophoric DOM (CDOM) absorbs ultraviolet (UV) light efficiently and is thus highly photoreactive in sunlight (Amon & Benner, 1996; Cory et al., 2014; Mann et al., 2012; Stubbins et al., 2010). When photooxidation results in the complete transformation of DOC to DIC or CO_2, it is called photomineralization.

In lakes and reservoirs, there is some convergence among existing estimates of photooxidation and photomineralization, with studies showing that these processes account for 9%–12% of DIC and/or CO_2 production in lakes and reservoirs locally, consumption of up to 11% of the DOC, and 10% of total lake CO_2 emissions globally (Allesson et al., 2020; Bertilsson & Tranvik, 2000; Granéli et al., 1996; Koehler et al., 2014). In rivers, it remains unclear whether photooxidation is a meaningful DOC consumption process, in part due to the dearth of studies that quantify riverine photooxidation (Bowen, Kaplan, et al., 2020; Bowen, Ward, et al., 2020; Cory et al., 2014; Gao & Zepp, 1998; Osburn et al., 2009; Selvam et al., 2019). Studies have focused on photooxidation fluxes in coastal river plumes or estuaries (Aarnos et al., 2018; Amon & Benner, 1996; White et al., 2010), which are fundamentally different from inland streams and rivers, in terms of water clarity and discharge as well as hydraulic and geomorphic properties like depth, width, and channel structure. Work in a temperate, canalized and turbid estuary, with properties more akin to a river channel than the river plume, suggests photochemistry removes less than 1% of DOC during estuarine transport in the Tyne estuary (Stubbins et al., 2011).

Most riverine photooxidation studies have relied on utilizing laboratory-based batch photodegradation experiments (Gao & Zepp, 1998; Niu et al., 2019; Opsahl & Benner, 1998; Shiller et al., 2006; Xie et al., 2004), which are useful for elucidating CDOM character and associated degradation mechanisms and optimized rates, but often do not account for turbidity, canopy shading, or water residence times. Higher turbidity, canopy shading, and short water residence times limit both the availability of incoming light as well as the time available for photochemical reactions to take place, and have generally not been accounted for in most laboratory experiments or extrapolations of laboratory rates to riverine systems (Macdonald & Minor, 2013). Existing studies that do calculate *in situ* riverine photooxidation rates across watersheds are focused in Arctic environments. For example, Cory et al. (2014) found that 70%–95% of water column mineralization was via photooxidation in Arctic lakes and rivers, though of the total watershed photooxidation, only 9% took place in rivers, with the remainder in lakes. Their study did not consider the proportion of total DOC flux that was mineralized biologically or photochemically.

The drivers of the magnitude of photooxidation and photomineralization fluxes can be conceptualized as the interplay between reaction and transport rates. Reaction rates are determined by the availability of light and DOC, and the chemical composition of the DOC. Photooxidation is dependent on the intensity and duration of incoming solar irradiation, mainly in the UV-A, UV-B, and visible light ranges of the spectra (approximately 280–600 nm) (Bowen, Kaplan, et al., 2020; Mopper et al., 2015; Vähätalo et al., 2000). In forested environments, incoming solar irradiation can be physically blocked from entering the water column by the tree canopy cover, which can vary substantially by season in temperate rivers due to the prominence of deciduous tree species (Detenbeck et al., 2016; Julian et al., 2008) (Figure 1). Once in the water column, incoming solar irradiation is attenuated with depth by suspended sediment (SS), including abiotic mineral detritus (tripton) and phytoplankton (Phlips et al., 1995), water (Buiteveld et al., 1994), and CDOM (Kirk, 1994). The combined impacts of these factors on light attenuation across relevant wavelengths is measured with a vertical attenuation coefficient (Davies-Colley & Nagels, 2008; Gareis et al., 2010; V.-Balogh et al., 2009). CDOM's ability to absorb light, which is dependent on its composition, is measured by an absorption coefficient, and impacts both how susceptible CDOM is to photooxidation as well as how efficiently it attenuates light within the water column (Hansen et al., 2016) (Figure 1). The ability for CDOM molecules to react with the photons of UV light absorbed and thus undergo photooxidation is dependent
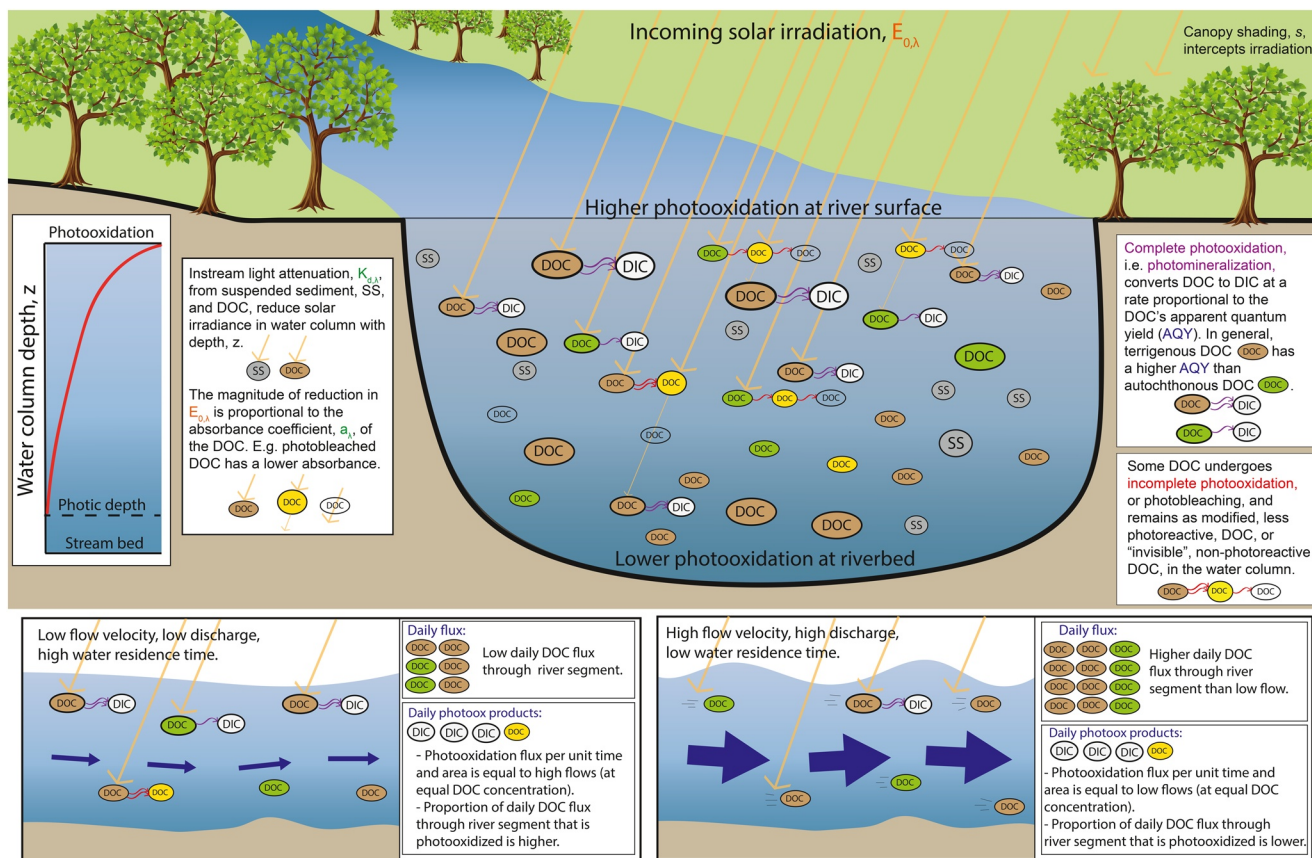
Figure 1. Conceptual model of photooxidation reaction rate controls (top panel) and transport rate controls (bottom panels). Top panel shows the cross-section of a river water column, with complete and incomplete photooxidation of terrigenous (brown) and autochthonous (green) dissolved organic carbon (DOC) shown. The by-product of partial or incomplete photooxidation, bleached DOC, is shown in yellow if it is still capable of absorbing some light, and as transparent "invisible DOC" if it does not absorb any light. Incoming solar irradiation is represented by orange arrows, and attenuation by tree canopy, DOC or suspended sediment (SS) is shown either as a termination of the arrow or a decrease in arrow size. At the far left, a photooxidation depth profile is shown, indicating the photic depth, beyond which no light penetrates and photooxidation fluxes are zero. The bottom left panel shows a stream with a low flow velocity and is therefore associated with a lower daily DOC flux. The bottom right panel has a higher flow velocity and higher daily DOC flux. Both systems have the same DOC concentration and light attenuation, and therefore the same daily areal photooxidation flux, but the proportion of the total daily DOC flux transported through the river segment, that is photooxidized is higher in the left panel.

on the apparent quantum yield (AQY), which for DIC photoproduction from DOC decreases exponentially as wavelength increases (Aarnos et al., 2018; Cory et al., 2014; Koehler et al., 2014, 2016). As with absorption, AQY is dependent on the composition of the CDOM. For example, allochthonous CDOM, which is terrigenous in origin and tends to have a high aromaticity, is usually highly photoreactive, while less terrestrial, more autochthonous CDOM in coastal waters and lakes is often less photoreactive (Bertilsson & Tranvik, 2000; Logozzo et al., 2021; Stubbins et al., 2011; Ziegler & Benner, 2000) (Figure 1). Complete photooxidation, that is, photomineralization, converts CDOM to DIC, potentially supporting CO_2 emissions. Photobleached DOC is less susceptible to produce CO_2 compared with DOC that has not been exposed to sunlight yet (Berggren et al., 2018; Miller & Zepp, 1995).

Transport rates deal primarily with the time available for DOC to be photooxidized within a given river reach, which is dependent on the physical hydrology. Streams with high water velocities tend to have high discharges (flows) and short water residence times, and thus less time is available for reactions to take place (Brinkerhoff et al., 2021; Raymond et al., 2016). Both classical and modern research in inland waters has shown that the relative proportion of a parcel or pulse of a constituent that is transformed or eliminated from the water column is inversely related to the water residence time (Maavara et al., 2020; Vollenweider, 1975). In the case of photooxidation in rivers, the absence of *in situ* studies that quantify the relative proportion of DOC that is mineralized photochemically represents a major shortcoming in our

understanding of this process at watershed scales. While lake and lab-based batch experiments can provide preliminary indicators of the magnitudes of photooxidation fluxes in rivers, these types of studies do not account for the short transport timescales. Although losses of photoreactive DOC within river systems have proved difficult to assess, there is a wealth of evidence that photoreactive DOC escapes rivers to the oceans. For instance, many studies report high export of CDOM and photolabile DOC to the oceans, suggesting that rivers in general are poor photoreactors of DOC (Spencer et al., 2013; Vodacek et al., 1997; Yoon et al., 2021). Our ability to quantify the relative importance of photomineralization as a DOC sink remains limited if it is not calculated in the context of the flux or concentration of DOC through a river reach over timescales of interest (Figure 1).

In this study, we develop a spatially explicit model of complete DOC photooxidation to DIC, that is, photomineralization, for the riverine reaches of the Connecticut River Watershed (CRW), a temperate river basin in the northeastern United States and southern Canada. Yoon et al. (2021) suggested there is potential for a large flux of photolabile DOC to escape the CRW annually, suggesting low photomineralization, but it remains unclear how much is photomineralized within the watershed itself. These findings, combined with the observations in existing literature that photomineralization fluxes typically only exceed ~10% of the total DOC consumption in systems with long water residence times like lakes and coastal plumes, or in regions with low canopy cover (e.g., Arctic environments), lead us to hypothesize that photomineralization is a minor process in temperate rivers where water residence times are low and canopy cover is high. Our model explicitly accounts for reaction and transport rates by solving the spectrally resolved photomineralization formulation for modeled DOC concentrations in each reach of the CRW across a range of flow conditions, stream orders and sizes, and seasons. We develop the model with the intent of testing the hypothesis that photomineralization is a negligible DOC sink across all conditions relative to the daily DOC fluxes through individual stream reaches and within the whole watershed's combined riverine segments. Thus, in situations where data are scarce or assumptions need to be made, we specifically make decisions that will result in higher calculated photomineralization fluxes, and further test these assumptions in a sensitivity analysis. We utilize field measurement data gathered throughout the CRW to parameterize our model. This model is the first to quantify both reaction and transport rates as photomineralization drivers across an entire watershed's river reaches for the observed ranges of flow conditions and seasonality parameters. Our model specifically takes into consideration water residence times across a range of flows in each river reach. It also accounts for seasonal changes to canopy cover. The scale and resolution of data our model can generate therefore enables us to contextualize the importance of photomineralization across continua of hydrological and biogeochemical conditions previously impossible with localized laboratory experiments and field sampling campaigns.

2. Materials and Methods

2.1. Overview

In this section, we briefly describe the Connecticut River Watershed characteristics and data collection used to build the photomineralization model (Section 2.2). We then explain how the watershed network is discretized and how hydrological parameters including flows, water residence times, and stream depths and widths are modeled (Section 2.3). Section 2.4 details the photomineralization model itself, including various metrics used to quantify the relative importance of photomineralization rates, and Section 2.5 summarizes model assumptions and details the sensitivity analyses performed.

2.2. Study Location and Data Collection

We focus our study on the Connecticut River Watershed (CRW), a 29,200 km^2 predominantly forested river basin, which empties into Long Island Sound (Figure S1). Grab sample collection of DOC concentrations and absorbance was primarily conducted at 13 sites on 1st- to 7th-order streams in two sub-watersheds: The Farmington River watershed in northwestern Connecticut, and the Passumpsic River watershed in northeastern Vermont (Figure S1), at a frequency of at least biweekly, between 2015 and 2017. Additional synoptic data was collected at the mouths of 5th- and 6th-order watersheds throughout the basin as well as on the 8th-order Connecticut River mainstem (Figure S1) on 2–32 occasions. Samples were analyzed for

DOC concentrations (TOC-vCPH with TNM-1; Shimadzu Corporation; Kyoto, Japan) and UV-Vis absorbance at 1 nm intervals from 200-800 nm. Full method details are available in Hosen et al. (2021). All sites were located at existing USGS monitoring sites where discharge (Q) data is reported online (USGS, 2020).

2.3. Watershed Hydrological Modeling

The CRW is discretized into 98,254 reaches according to the NHD Plus High Resolution (HR) data set (Buto & Anderson, 2020; Moore et al., 2019). For the purposes of this analysis, which is focused on riverine photomineralization only, any reaches identified in NHD Plus HR as a lentic water body (i.e., a lake, pond, or reservoir) determined based on whether they had a nonzero lentic water body surface area attribute value ("WB_AreaSqKm") were excluded (i.e., we assume that anything classified as having a lentic water body area of zero, or left empty, was a lotic reach). Thus, 75,018 river reaches were included in this analysis, with an average length (L_r) of 511 m. In general, NHD Plus HR reaches are discretized based on when new tributaries join or a waterbody intersects the river. As a result, rivers of all stream orders are broken into multiple reaches, including first order tributaries (which are frequently segmented by ponds). Discharges ($m^3 s^{-1}$) and hydraulic residence times (HRT, days) were calculated according to the method of Brinkerhoff et al. (2021) at four different "characteristic discharges" (Q_2, Q_{15}, Q_{50}, Q_{98}), which refer to the streamflows for each reach that exceeds that percent of the time. Q_{50} represents median annual flows calculated specifically for each reach, while Q_2 and Q_{98} represent extreme flood and low-flow events at the tail ends of the observed record, respectively. Due to an inability to generate robust width relationships that were applicable across the 75,018 river reaches in the model domain from the comparatively small number of available discharge rating curves at gauge stations within the CRW, discharge-dependent reach segment widths (w, in meters) are calculated using the empirical relationship from Raymond et al. (2013) from 9811 USGS stream gauging stations across the United States:

$$\ln\left(w\right) = 0.51\ln Q + 1.86 \tag{1}$$

Volume (vol, in m^3) is back-calculated using:

$$vol = \left(HRT \times 86400\right) \times Q \tag{2}$$

where HRT is in days and Q is in $m^3 s^{-1}$. Depth (z, in m) can then be calculated as the missing dimension using vol, L_r and w.

2.4. Watershed Photomineralization Model

Concentration-discharge (C-Q) relationships are conventionally used to predict concentrations in situations where Q data is available in continuous time series and C is available only intermittently (Hirsch et al., 2010). In the case of DOC, C-Q relationships tend to be fairly robust and follow predictable, repeatable trends (Creed et al., 2015; Rose et al., 2018). The use of a specific discharge, q, calculated by dividing Q for each reach by the upstream watershed area, can be useful for developing C-q relationships that are more broadly applicable than conventional C-Q across a large range of stream orders and sizes. DOC concentrations in mg L^{-1} are calculated using power laws with q ($m^3 s^{-1} km^{-2}$). For upstream watershed areas larger than 10 km^2, the following equation was generated from measurements collected within the CRW (sample collection described in Section 2.2; $n = 1,142$):

$$DOC = 7.413q^{0.1668}; R^2 = 0.15 \tag{3}$$

To enable the model to more realistically predict lower concentrations in small headwater streams, we fit a separate power law for reaches with upstream watershed areas less than 10 km^2 using the CRW measurement sites that meet this criterion ($n = 341$):

$$DOC = 9.9q^{0.2849}; R^2 = 0.32 \tag{4}$$

These relationships reproduce average concentrations across the spectrum of discharges. These trends account for the chemostasis trends typically observed in higher order streams (Creed et al., 2015), and the concentrating relationship at low and medium flows, and switch to chemostasis across all order streams at high flows, as observed for DOC in the CRW by Hosen et al. (2021) (shown in Figures 3d–3f).

Complete photooxidation of DOC to DIC (i.e., photomineralization, ψ), in each river reach is based on the spectrally resolved formula (Cory & Kling, 2018; Koehler et al., 2014):

$$\psi = \int_{0}^{z_{\text{stream}}} \left(\int_{\lambda_{\text{min}}}^{\lambda_{\text{max}}} E_{0,\lambda} a_\lambda e^{-\left(K_{d,\lambda} z\right)} \phi_\lambda d\lambda \right) dz \tag{5}$$

where λ_{min} and λ_{max} are the maximum and minimum wavelengths (280–600 nm), z_{stream} is the water column depth (m), $E_{0,\lambda}$ is the daily downwelling irradiance (mol photons m^{-2} day^{-1} nm^{-1}), a_λ is the Napierian CDOM absorption coefficient (m^{-1}), $K_{d,\lambda}$ is the vertical attenuation coefficient for downwelling irradiance in the water body (m^{-1}), z is the depth (m), and ϕ_λ is the apparent quantum yield (AQY, mg-C (mol photons)$^{-1}$ nm^{-1}), which describes the photoreactivity of the DOC in each reach by quantifying the complete photomineralization of DOC to DIC. ψ is calculated in units of mg-C m^{-2} day^{-1}, and converted to mg-C day^{-1} by multiplying by reach length and width.

Average monthly $E_{0,\lambda}$ values from wavelengths 280–600 nm for the CRW were generated using the SMARTS2 model, version 2.9.8 (Gueymard, 1995, 2019). SMARTS2 can be programmed with 30 user-defined parameters and was used to output global photon irradiance (mol photons m^{-2} day^{-1} nm^{-1}) at 1 nm resolution ("global" meaning integrated over the whole sky, accounting for both direct normal irradiation and diffuse horizontal irradiation). SMARTS2 outputs location- and time-specific solar spectra for a cloud-free atmosphere. In order to approximate average monthly irradiance for the entire CRW, we utilized a standard United States atmosphere, and input a central latitude, longitude and average watershed elevation for the CRW, and output spectra for the 15th day of each month, which we assumed to be an average approximation of the monthly conditions. To calculate the total daily irradiance, we output irradiance from SMARTS2 at solar noon, solar noon plus two hours, solar noon minus two hours, sunrise and sunset, and then integrated these spectra over the entire day using sunrise and sunset times output from the model, thus accounting for the entire diel variation in irradiance. In order to simplify the integration in Equation 5 and reduce computational demand, we approximate each monthly $E_{0,\lambda}$ spectra using a 2-term Fourier model ($R^2 = 0.97$). Details related to this approximation, the SMARTS2 input parameters used and the magnitude of the $E_{0,\lambda}$ spectra can be found in the Supplementary Material, Section S1 and Figure S2. Additionally, we do not account for ice cover assuming that photochemistry occurs all winter with the same efficiency as during ice-free months. This approach was taken to maximize potential DOC photodegradation losses in accordance with our testing of the hypothesis that photomineralization is a negligible DOC sink.

Throughout the paper, we present a matrix of results from March, June, and December, at the four different characteristic discharges (Q_2, Q_{15}, Q_{50}, Q_{98}), thus generating 12 model scenarios. The months chosen represent the maximum (June), minimum (December), and approximate mean (March) $E_{0,\lambda}$ values for the year. This matrix approach allows us to test the full range of possible flow conditions against the full range of possible incoming solar irradiation conditions. Thus, while in reality we would expect extremely low flows (e.g., Q_{98}) to occur mainly in summer, for example, our model setup enables calculation of these flows in any months to identify possible parameter combinations that could drive high photomineralization fluxes. The Q_{15} flow scenarios represent the approximate "effective discharge" for DOC for an 8th order New England watershed such as the CRW, as identified in Raymond et al., (2016) (they provide estimate as a flow percentile of 83%, approximately equivalent to our flow exceedance percentage of 15%). The effective discharge describes the flow at which the flux of DOC is the highest, or the flow where the "most work" is being done in terms of exporting DOC (Doyle et al., 2005).

$E_{0,\lambda}$ was further refined to account for seasonal canopy shading by multiplying by the shading coefficient S_{can}, a unitless ratio of the incoming radiation above the canopy to the ratio that reaches the stream surface ($S_{\text{can}} = 1$ indicates no canopy shading, 0 = complete shading) (Julian et al., 2008). We trained a bagged trees regression model (100 trees, optimized minimum leaf size of 5) using 5-fold holdout cross validation for winter and summer canopy cover based on 301 canopy gap photographs taken throughout the CRW

(Creech et al., 2021). The model's training variables were stream order, land cover (forested vs. unforested), and stream width. The trained winter model was then applied to all NHD Plus HR reaches for November-April, and the summer model applied to all reaches for May–October. The summer canopy model predictions had a root mean square error (RMSE) of 10.3%, while the winter model's RMSE was 6.6%.

Using 1,142 field sample measurements from the CRW, the following regression was established to estimate the decadic absorption coefficient at 350 nm (a_{350}) from measured DOC concentrations in mg L^{-1}:

$$a_{350} = 1.185\,DOC - 0.5671; R^2 = 0.78 \tag{6}$$

where a_{350} is in m^{-1}. We then convert a_{350} to the Napierian absorption coefficient by multiplying by ln(10). From the same field samples, we computed an average exponential slope coefficient, $s_{280-450}$, for the 280–450 nm band, of 0.017 nm^{-1} (standard deviation = 0.0013 nm^{-1}). Hence, the Napierian absorption coefficient at all wavelengths, inserted into Equation 5, is computed using:

$$a_{\lambda} = a_{350}e^{s_{280-450}(350-\lambda)} \tag{7}$$

$K_{d,\lambda}$ at all wavelengths is assumed to be equal to a_{λ} (i.e., we assume that light is attenuated only by CDOM). Light attenuation due to water accounts for <1% of calculated CDOM attenuation at all wavelengths and flow conditions (Stubbins et al., 2006) and so could be neglected. Particles (i.e., total suspended solids, TSS) in the water column can be photoreactive (Helms et al., 2014). However, particle and particulate organic matter photoreactivity is not addressed here as we focus upon the potential for sunlight to remove DOC from the water column. Particles may also indirectly impact photoreactions that occur in the water column as they absorb and scatter light, potentially reducing the photons available for absorbance by CDOM. Scattering may lead to the reflection of photons out of the water (Novo et al., 1991) while absorbance by particles can compete with CDOM for incoming photons within the water column (Stubbins et al., 2006, 2011). The net effect of particles in the water column is therefore likely a reduction in DOC photomineralization. In the current study, we aim to specifically assess whether photochemistry is quantitatively important to the loss of DOC during transport. Therefore, we omit particles from our light calculations, so that all available photons in the model interact only with CDOM (Stubbins et al., 2011).

Using Napierian a_{420} (in nm), we calculate AQY at 300 nm (ϕ_{300}) using the linear regression determined by Koehler et al. (2016):

$$\phi_{300} = 55.5 \times 10^{-6} \, a_{420} + 528.1 \times 10^{-6}; \quad R^2 = 0.64 \tag{8}$$

where ϕ_{300} is calculated in mol C (mol photons)$^{-1}$, and subsequently converted to mg C (mol photons)$^{-1}$. Using an exponential AQY slope (s_{AQY}) across wavelengths of 0.017 nm^{-1}, determined from spectra presented in Koehler et al. (2016), the following generalized equation for ϕ_{λ} is obtained:

$$\phi_{\lambda} = \phi_{300}e^{s_{AQY}(300-\lambda)} \tag{9}$$

The photomineralization uptake velocity, υ_f, in m day^{-1}, is calculated by dividing the surface area-normalized photomineralization flux (mg-C m^{-2} day^{-1}) by the DOC concentration (in mg L^{-1}) multiplied by 1,000 (to convert L to m^3) (Stream Solute Workshop, 1990; Wollheim et al., 2018). When applied to dissolved constituents, υ_f describes the first order rate of reaction relative to an interface (i.e., the water surface), allowing for variability with changing concentrations (Wollheim et al., 2018).

In each reach of the CRW, we calculate a per-reach elimination, R_r (unitless), describing the proportion of available DOC, that is, photomineralized:

$$R_r = 1 - \exp\left(\frac{-\upsilon_f}{H_l}\right) \tag{10}$$

where H_l, the hydraulic load (m day^{-1}), is calculated according to:

$$H_l = \frac{Q}{L_r w} \tag{11}$$

where Q is in m^3 day^{-1} and reach length, L_r, and width, w, are in m (Mineau et al., 2016). R_r varies between 0 and 1, where 0 indicates none of the reach DOC is photomineralized, and a value of 1 indicates 100% of the DOC in the reach is photomineralized. R_r is equivalent to the relative uptake rate, that is, the proportion of the DOC flux through a reach, that is photomineralized. Equation 10 can be thought of as an indicator of the relative importance of reaction rates, represented by υ_f, to transport rates, represented by H_l. In reaction dominant systems, R_r is closer to 1, while in transport dominant systems, R_r is closer to 0. To precisely compare elimination across reaches of different lengths, we present the reach length-normalized R_L:

$$R_L = \frac{R_r}{L_r} \tag{12}$$

Using R_L we can approximate the overall proportion DOC that is photomineralized over any length of river segment (Table S2).

2.5. Model Assumptions and Sensitivity Analysis

To test the hypothesis that photomineralization is negligible as a DOC sink in temperate rivers, the conservative assumptions previously detailed are designed to maximize the photomineralization fluxes. These assumptions are:

1. Total suspended sediments (TSS) do not contribute to light attenuation.
2. Pure water, which has an absorbance of <1% of CDOM, does not contribute to light attenuation.
3. Ice cover in winter months does not impact photomineralization.
4. Cloud cover is not included.
5. We use a matrix of flow conditions and seasonality to quantify the full range of observable flow conditions in all seasons. Rather than restricting high flows to the snowmelt, or low flows to summer drought, for example, we assume all flows are possible across all seasons.

To test the sensitivity of the calculated photomineralization fluxes to changes in parameters in Equation 5, as well as identify absolute maximum possible photomineralization flux, we perform a sensitivity analysis for the model output for the month of June, which has the highest $E_{0,\lambda}$. Specifically, we perform the following scenarios:

1. $K_{d,\lambda} = 0$, for Q_2, Q_{50}, and Q_{98} flows
2. DOC concentrations calculated with Equations 3 and 4, multiplied by factors of 2, 4, and 10, for Q_2 (highest) flows
3. Stream depth = infinite for Q_2, Q_{50}, and Q_{98} flows (i.e., assume every photon is absorbed by CDOM and thus photomineralization is determined by the AQY).
4. AQY calculated with an alternate expression from Koehler et al. (2016), for Q_2, Q_{50}, and Q_{98} flows:

$$\phi_{400} = 6.6 \times 10^{-6} \, a_{420} + 126.8 \times 10^{-6}; R^2 = 0.26 \tag{13}$$

5. No canopy cover across the entire watershed, for Q_2, Q_{50}, and Q_{98} flows.

The full results of these sensitivity scenarios can be found in Supplementary Material, Section S2, and Tables S3 and S4.

3. Results and Discussion

In the following two sections we consider the controls on photomineralization loss both from the standpoint of the drivers of the absolute areal rates (Section 3.1), including discussion of uptake velocities (υ_f), and in terms of the drivers of DOC loss relative to the available DOC flux through a reach or the entire river portion of watershed, that is, the relative uptake rate, or R_r (Section 3.2). Each metric has its own

advantages: Areal DOC rates and uptake velocities enable us to compare reaction rates with other ecosystem fluxes or water body types, in the absence of transport controls, while relative or percent DOC uptake allows us to consider the impact of photomineralization on the export of DOC through a reach or watershed, taking into consideration both reaction and transport rates and timescales. Uptake velocities, which describe the areal rate (mg-C m^{-2} day^{-1}) normalized by the DOC concentration, assume that the reaction occurs according to first order kinetics at the water-air or water-benthic sediment interface (Wollheim et al., 2018). For example, in the case of suspended particles, v_f is equivalent to a settling velocity, and in the case of gases, v_f is equivalent to piston velocity. In the case of photomineralization, the input of light occurs across the air–water interface, but the photomineralization occurs within the water column; thus, in addition to being dependent on the concentration, photomineralization rates are also dependent on the water column depth. In Section 3.1, we therefore present photomineralization v_f in order to facilitate comparison with other riverine water column processes that are more conventionally represented as being relative to an interface, but further describe the role of the added depth dependence on v_f.

3.1. Areal Photomineralization Rates and Uptake Velocities

Across the 75,018 CRW river reaches included in our model, our output predicts mean photomineralization fluxes ranging from 1.16 mg-C m^{-2} day^{-1} in low flow (Q_{98}) winter conditions to 18.33 mg-C m^{-2} day^{-1} in high flow (Q_2) summer conditions (Table 1). Overall drainage network average fluxes at median (Q_{50}) flows range from 2.45 to 13.90 mg-C m^{-2} day^{-1}, depending on season, and thus represent the range of fluxes observed in the most usual flow conditions throughout the watershed. Maximum values were as high as 71.42 mg-C m^{-2} day^{-1} (Table 1). These rate estimates align with existing local measurements in freshwater lakes. Allesson et al. (2020) found average July–August rates of 8.4–21.4 mg-C m^{-2} day^{-1} in 77 Norwegian and Swedish lakes between 57°N and 64°N, accounting for 2% daily loss of the standing stock of DOC. Also in Swedish lakes, Koehler et al. (2014) determined fluxes of 15.4–41.9 mg-C m^{-2} day^{-1}. Only the upper range of our estimates (Table 1) overlaps with the 35.8–296 mg-C m^{-2} day^{-1} fluxes found in high-Arctic rivers in the summer in Cory et al. (2014). These differences in magnitude are potentially accounted for by the long daylight hours in the Arctic summer sampling period, the absence of significant canopy shading in tundra landscapes, and more photoreactive Arctic DOM pools (i.e., higher AQYs). In major river plumes to coastal oceans, Aarnos et al. (2018) determined fluxes of 624–1,884 mg-C m^{-2} day^{-1}, and Amon and Benner (1996) calculated a flux of 118 mg-C m^{-2} day^{-1} in the Amazon River plume, substantially exceeding the inland temperate riverine fluxes we present here. The lack of canopy cover in open ocean river plumes, as well as longer water residence times, deep water columns, and high DOC availability, likely drive the substantially larger photomineralization magnitudes observed in these systems.

In the absence of canopy and cloud cover, our model is constructed such that the absolute areal photomineralization fluxes (mg-C m^{-2} d^{-1}) are dependent on the DOC concentration (which influences absorbance and K_d), AQY, and water column depth (Figure 2). Furthermore, because DOC also limits light penetration, at each DOC concentration, there is a critical depth above which approximately >95% of incoming light in the UV spectrum is attenuated. By approximating this threshold (indicated by the red curve along the shoulder of the plane in Figure 2), we can generate a relationship predicting riverine photic depth, z_{photic}, as a function of DOC concentration:

$$z_{photic} = 3.5\,DOC^{-1.25} \tag{14}$$

According to this expression, due to an increase in both DOC concentration and depth with increasing Q, at Q_2, Q_{50}, and Q_{98} flows, there are 15%, 3% and 1.5% of flowing reaches in the CRW where no light penetrates through the water column to the stream bottom (z_{stream}), respectively, distributed across all stream orders (Note that the number of reaches that run dry increases as flows decrease, and are not included in these percentages).

When z_{stream} is equal to z_{photic}, the photomineralization uptake velocity, v_f, is maximized for a given concentration; we refer to this situation as Condition (i) (Figure 2). A higher uptake velocity indicates a higher areal uptake rate for a given DOC concentration. According to Equation 14, the highest v_f values that can
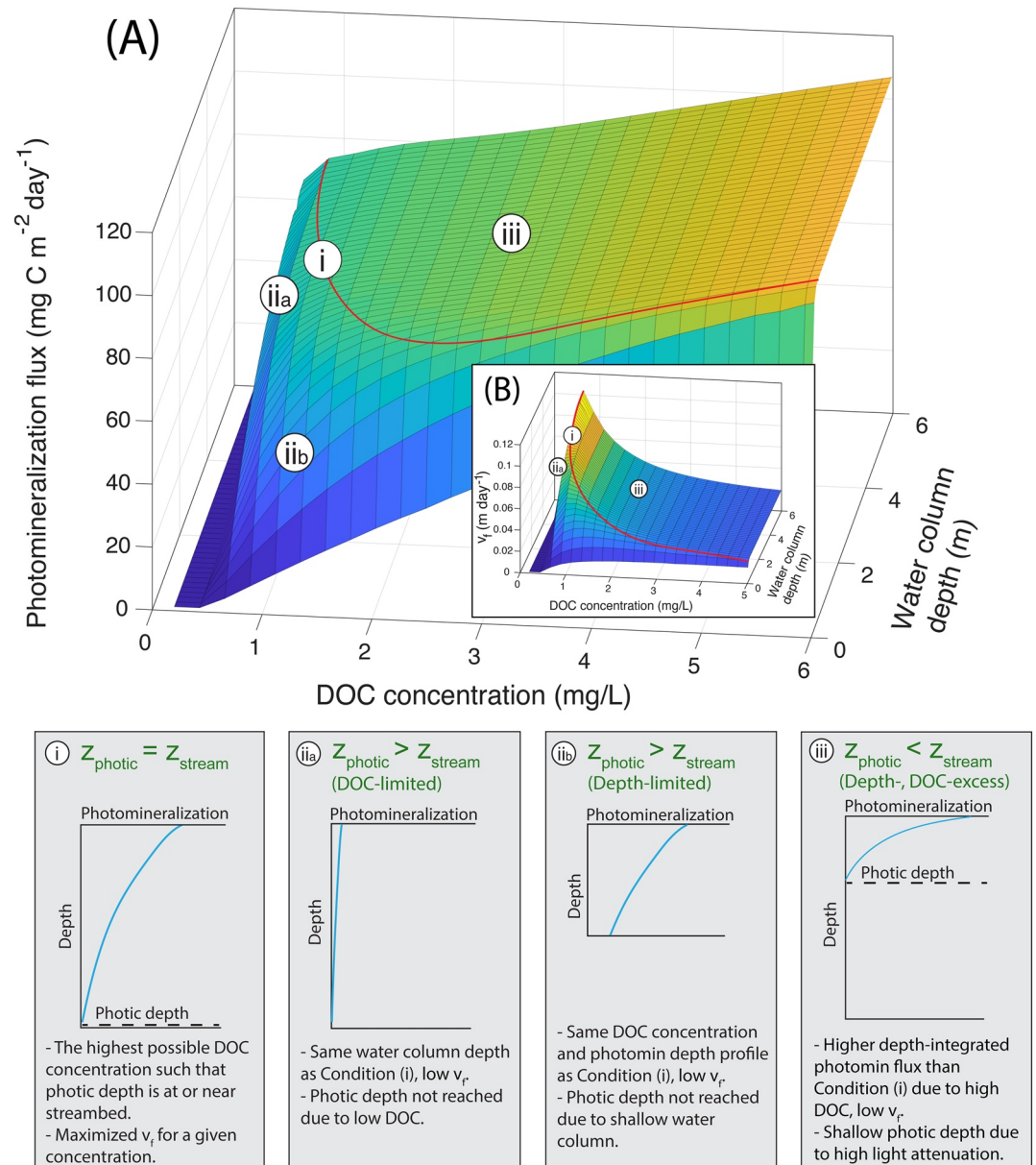
Figure 2. (a) June photomineralization flux as a function of dissolved organic carbon (DOC) concentration and total water column depth. (b) Uptake velocity, v_f, as a function of DOC concentration and total water column depth. In both panels, the effects of canopy shading are excluded in order to emphasize water column DOC and depth drivers. The shapes of the planes are consistent across seasons, only the magnitude of the photomineralization flux decreases in other months due to differences in downwelling irradiation (Table 1). In panel (a), the red curves indicate the shoulder above which added water column depth does not increase the magnitude of photomineralization and thus represents the photic depth at different DOC concentrations, fit with Equation 14. In panel (b), the red curve also corresponds to the maximized v_f at each DOC concentration and depth. The panels (i), (ii$_a$) (ii$_b$), and (iii) represent the generalized photomineralization conditions possible in the water column, as indicated by their marked position on the plane.

occur within Condition (i) require concentrations between 0.75 and 1 mg/L and z_{stream} >5m. These low concentrations and relatively high depths are the conditions where the ratio of DOC availability to DOC light attenuation from self-shading (when the absorbance of light by CDOM also limits the availability of light needed for photomineralization of CDOM to occur) are maximized, enabling the highest areal photomineralization flux per unit DOC. In the CRW, mean uptake velocities at median flows range from 9.1×10^{-4} –0.0054 m day^{-1} (Table 1). Across all flows, while Condition (i) situations are achieved throughout the
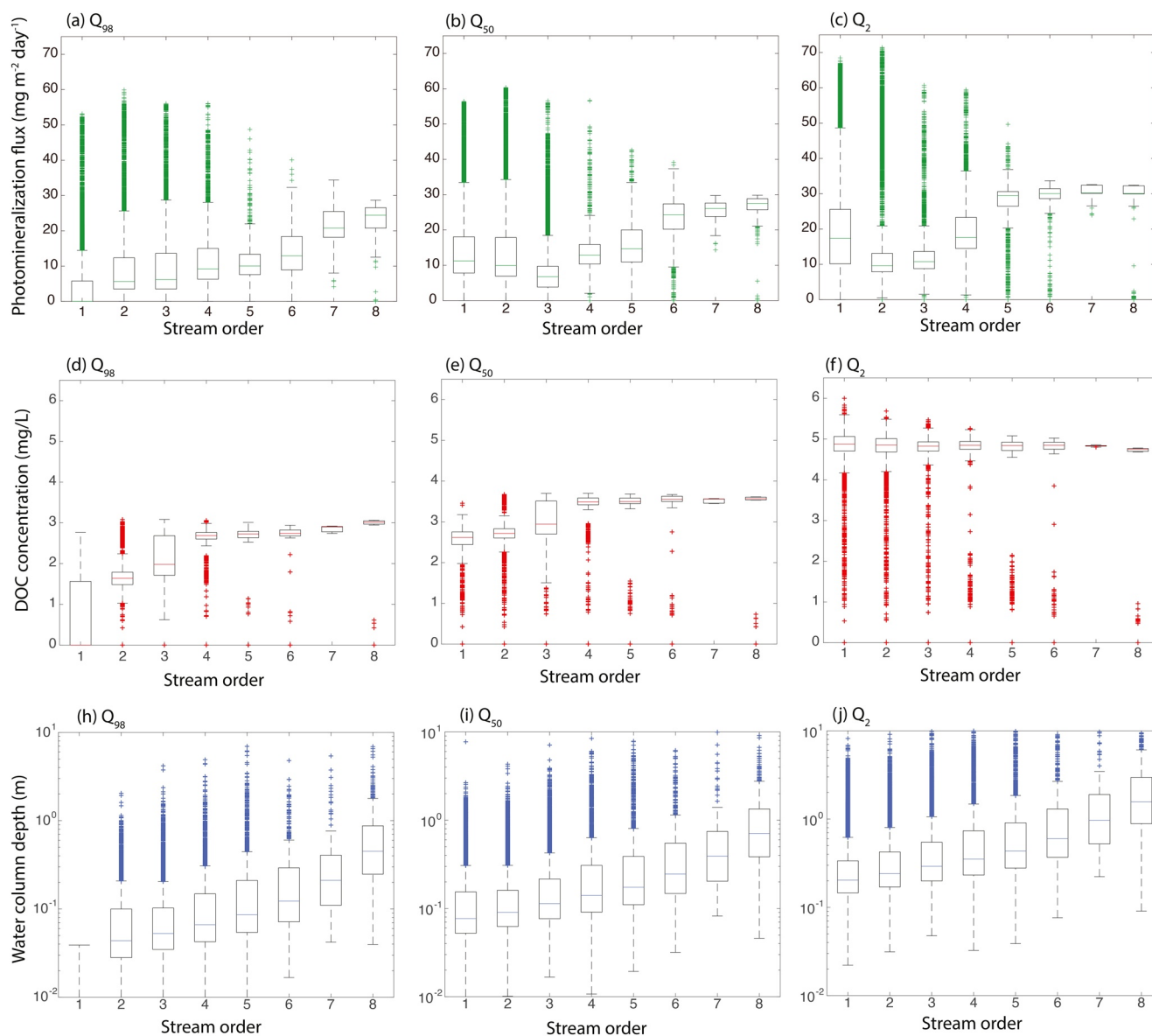
Figure 3. (a–c): June surface area-normalized photomineralization fluxes for Q_{98}, Q_{50}, and Q_2 flows for all reaches in the Connecticut River Watershed (CRW), including impacts of canopy cover. An analogous box plot but without the effects of canopy shading can be found in Figure S3. (d–f): Distributions of DOC concentrations (mg/L) across stream orders for Q_{98}, Q_{50}, and Q_2 flows for all reaches in the CRW throughout the year. (h–j): Distributions of water column depths across stream orders for Q_{98}, Q_{50}, and Q_2 flows for all reaches in the CRW throughout the year. In all panels, middle line indicates median, box edges are 25th and 75th percentiles, and the whiskers extend to the most extreme values not considered outliers. Note the log scale on the *y*-axis in panels h–j. Depth outliers above 10 m are not shown for clarity.

waters, the DOC concentrations and depths needed to achieve the maximum Condition (i) v_f values of 0.12 m day^{-1} (Figure 2b) never occur, and v_f never exceeds 0.043 m day^{-1} (Table 1).

Compared with uptake velocities for other riverine reactions, photomineralization v_f are exceptionally low and are not much greater than conservative tracers such as chloride, which have an assumed v_f equal to 0. Ensign and Doyle (2006) found uptake velocities for ammonium, phosphate, and nitrate uptake of 3–15, 1.3–8.6, and 0.7–6.3 m day^{-1}, respectively, and Mulholland et al. (2008) similarly found uptake velocities for nitrate removal in rivers of 0.3–2.7 m day^{-1}, and 0.02–0.17 m day^{-1} for denitrification only. Mineau et al. (2016) found DOC uptake velocities of 0.25–41 m day^{-1} for simple labile compounds such as acetate, glucose and arabinose, and 0.003–10 m day^{-1} for leaf leachate-derived DOC. Wollheim et al. (2015) found

Table 1
River Photomineralization Fluxes, ψ, in mg-C m^{-2} day^{-1}, and Uptake Velocities, υ_f, in m day^{-1} Per Reach, For the CRW at Maximum, Minimum, Effective Discharge, and Median Flows and Downwelling Irradiance Conditions

Month	Parameter	Q_{98}		Q_{50}		Q_{15}		Q_2	
		ψ	υ_f	ψ	υ_f	ψ	υ_f	ψ	υ_f
March	Mean	3.48	0.0026	7.33	0.0027	10.26	0.0028	13.42	0.0028
	Median	2.12	0.0019	5.41	0.0021	7.86	0.0022	10.14	0.0021
	Max	35.48	0.016	37.63	0.014	40.25	0.020	42.73	0.017
June	Mean	7.10	0.0056	13.90	0.0054	17.13	0.0048	18.33	0.0039
	Median	4.41	0.0038	10.73	0.0041	13.90	0.0038	13.45	0.0028
	Max	59.90	0.038	60.33	0.043	64.84	0.039	71.42	0.039
December	Mean	1.16	8.7×10^{-4}	2.45	9.1×10^{-4}	3.46	9.4×10^{-4}	4.55	9.6×10^{-4}
	Median	0.69	6.1×10^{-4}	1.79	6.8×10^{-4}	2.63	7.2×10^{-4}	3.46	7.1×10^{-4}
	Max	12.28	0.0055	13.00	0.0047	13.88	0.0067	14.77	0.0058

bulk DOC removal uptake velocities averaging 0.039 m day^{-1} (with quartiles 0.036–0.041 m day^{-1}) for a much smaller (400 km^2) temperate watershed in New England. Given that the upper mean value for any month in our study is over an order of magnitude lower, and mean winter month values are over two order of magnitudes lower than Wollheim et al. (2015)'s bulk values, our findings indicate that photomineralization is not a consequential flux in lotic temperate forested systems like the CRW.

Condition (ii) (Figure 2) describes situations where $z_{photic} > z_{stream}$, characterized by lower areal photomineralization rates and lower υ_f than Condition (i), due to lower DOC concentration (substrate-limited Condition ii_a, as in Cory and Kling (2018)) or lower water column depths (depth-limited Condition ii_b, Figure 2). In substrate-limited Condition (ii_a), areal rates are limited by DOC availability: while light penetration into the water column is higher at these lower DOC concentrations, the magnitude of the photomineralization flux is limited by the availability of DOC, and thus the overall magnitude of depth-integrated photomineralization, as well as υ_f, are low. Depth-limited Condition (ii_b) is limited by water column depth; photomineralization depth profiles are "cut off" at the river bed, which is at a depth lower than the photic depth would be as predicted by Equation 14. Condition (iii) describes situations where photomineralization fluxes can be as high or higher than Condition (i), but the entire water column is not being used efficiently due to CDOM self-shading, and therefore deeper water columns do not result in higher areal fluxes. Condition (iii) therefore describes a situation with excess substrate and depth. Photomineralization fluxes increase at a slower rate with rising DOC concentrations than in both substrate-limited and depth-limited Condition (ii), and added water column depth does not contribute to increases in photomineralization as the photic depth has already been exceeded (Figure 2). According to our results, depth-integrated photomineralization fluxes continue to increase as DOC concentrations rise through concentrations typically observed in temperate rivers (>50 mg/L, see Supplementary Material Section S2), but occur progressively closer to the river surface. Our results show that maximum areal photomineralization fluxes occur in June and are maximized in water column depths of more than 2m (Table 1, Figure 2).

In order to better understand the frequency under which environmental conditions in temperate rivers maximize areal photomineralization fluxes or uptake velocities, we can look at trends in photomineralization by stream order and compare with DOC concentrations and stream depth distributions (Figure 3). Across all stream orders, DOC concentrations increase with higher flow. However, the direction of the photomineralization response to increasing DOC concentrations varies by stream order. The median surface area-normalized photomineralization is highest in 8th-order streams at all flows, due to a combination of lower canopy shading and reaches that occur within Condition (iii) (i.e., excess substrate and depth). Photomineralization fluxes in progressively lower stream orders increase as flows increase due to shifts from both depth- and substrate-limited Condition (ii) into Condition (i) (i.e., maximized υ_f) and Condition (iii) (excess depth and DOC), with median magnitudes in 5th–7th order streams nearing that of 8th order in Q_2 flows. In Q_{98} flows, 1st–4th order streams have DOC concentrations near those which would result
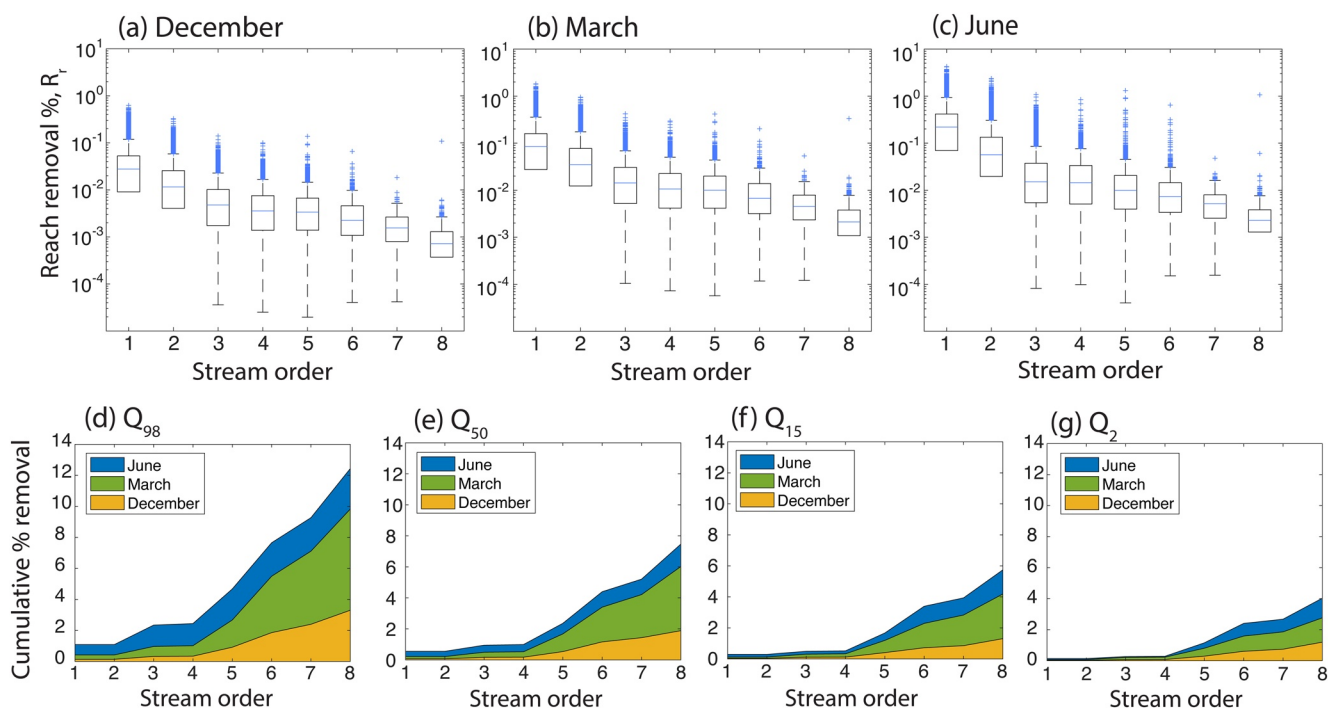
Figure 4. (a–c) Box plots of the reach removal efficiency (R_r, %) at Q_{50} flows for March, June, and December. (d–g) The cumulative percent removal of a pulse of dissolved organic carbon (DOC) that enters the river network in a 1st order stream and follows the longest path in the Connecticut River Watershed (CRW) through sequential stream orders, of maximum total length L_L (as in Table S2), for March, June and December at Q_{98}, Q_{50}, Q_{15}, and Q_2 flows.

in maximized photomineralization uptake velocities in Condition (i) reaches; however, although the DOC concentrations are near the optimum, these small systems are often more light-limited due to increased canopy cover, and are very shallow, and so are unable to support high photomineralization fluxes in excess of 10 mg-C m^{-2} day^{-1}. In other words, a small number of outliers in these low order streams follow v_f-maximized Condition (i), while the majority can be represented by depth- or substrate-limited Condition (ii). As both depths and DOC concentrations increase with flow, the maximum observed photomineralization fluxes are lower as DOC light attenuation grows and both Condition (i) and (ii) instances become Condition (iii). In 5th–7th order streams, rising discharges and associated depth and DOC concentration increases result in the switch from depth- or substrate-limited Condition (ii) to (iii), and $z_{stream} > z_{photic}$. The overall lack of meaningful change across flows in the magnitude of photomineralization in 8th-order streams reflects the chemostatic C-Q relationships typically observed for DOC in larger rivers (Creed et al., 2015) including the CRW (Hosen et al., 2021), which are captured in Equation 3. In other words, 8th-order streams have minimal change in photomineralization fluxes across flows because they exist in the excess substrate and depth Condition (iii) even in lowest flows, and given the small change in DOC concentration, are impacted mainly by changing depths, which have no impact within Condition (iii).

3.2. Relative Reach- and Watershed-Scale Riverine DOC Removal

At median flows, average per-reach photochemical processing of daily DOC fluxes (R_r) is 0.026%–0.18%, with expectedly higher R_r in summer months (Figures 4a–4c, Table S1). Including the effects of canopy cover, we find that 1st-order reaches have the largest R_r values, with R_r decreasing approximately exponentially in all flows and months as reach order increases (Figures 4a–4c, Table S1). High R_r in low order reaches are driven by low DOC concentrations and shallow water columns, enabling larger proportions of the available DOC to be photomineralized since there is little DOC to begin with and light does not need to penetrate into a deep water column to access it. However, even the most efficient 1st-order reaches only photomineralize an average of 0.58% of the DOC that passes through them during peak summer solar irradiance (Figures 4a–4c, Table S1). Eighth-order reaches, comparatively, rarely photomineralize more than 0.007% of

the DOC that passes through them. These trends indicate that transport rates substantially exceed reaction rates, and while overall daily photomineralization fluxes are comparable to lakes, the limited R_r reflects the magnitude of DOC moving through the system on a daily basis. In lakes, for the same reaction rates, we can expect higher R_r values due to longer water residence times and lower transport rates. We additionally note that reaches in the CRW remain transport dominated with regard to photomineralization across flows. Therefore, while the absolute areal rates we calculate per reach are comparable to lentic water bodies, the relative proportion of the daily DOC fluxes through reaches that undergo complete photomineralization only exceeds 1% in extremely low flows (e.g., drought conditions) in 1st order streams during peak summer irradiance.

To examine the whole-watershed cumulative impacts of complete photomineralization in rivers on DOC loss, we can consider the travel distance of a parcel of DOC from headwaters to the river outlet. For example, the longest route from the CRW headwaters to Long Island Sound that can be traveled is 611 km, not including lentic water bodies, with specific distance for each stream order (L_L) is given in Table S2. Using R_L and L_L we can calculate the maximum cumulative loss via photomineralization for a parcel of terrestrial DOC entering the watershed in a 1st order stream as it passes sequentially through stream orders 1 to 8 in the CRW (Figures 4d–4g). Using mean R_L values for each stream order and for any flow scenarios and season, and the reach lengths L_L given in Table S2, less than 12.5% of the original DOC mass is consumed before reaching the river outlet. Cumulative relative photochemical losses are highest in Q_2 flows in June (12.4% loss), whereas in December, cumulative riverine whole-watershed consumption is less than 4% in all flow conditions (1.2% in high flows). Thus, these results indicate that whole-watershed riverine photomineralization may become important only in peak summer severe drought conditions during low flows that occur less than 2% of the time, but that even DOC parcels following the longest possible flow path will only be photooxidized by at most 12.4%, and the absolute photomineralization flux will be the lowest of all flow conditions (Table 1). The mean travel distance for the CRW from headwater streams to the outlet (excluding travel through lentic water bodies) is 296 km, through all combinations of network connectivity. Thus, for flow ranging from Q_{98} to Q_{50}, average cumulative photomineralization loss of a DOC parcel is approximately 4%–6% in June, 3%–5% in March, and less than 1.5% in December. In reality these mean losses are likely much lower, given we do not account for cloud or ice cover or water column attenuation by suspended sediment. At high Q_2 flows, cumulative photomineralization never exceeds 2% following the average riverine watershed path length in any season, despite experiencing the highest absolute photomineralization fluxes. Comparatively, the bulk uptake of terrestrial DOC via any mechanism for an average flow path through a hypothetical forest 8th order New England watershed (Raymond et al., 2016), ranged from 56% at high flows to 85% at low flows. Based on this comparison, we can infer that the majority of whole-watershed riverine DOC removal occurs via bio-mineralization rather than photomineralization. Another way to consider the overall impact of photomineralization is to consider the impacts of photomineralization for the effective discharge for DOC, which for a watershed like the CRW is around Q_{15} (Raymond et al., 2016). At these flows, 5.7% of the DOC is removed following the longest flow length in June, and 1.3% in December.

The results of the sensitivity analyses performed additionally do not offer many convincing scenarios in which photomineralization represents a meaningful loss term relative to DOC fluxes (Supplementary Material Section S2, and Tables S3 and S4). The absence of canopy cover has the largest impact on both the absolute and relative photomineralization fluxes. In winter, canopy cover reduced the potential magnitude of photomineralization fluxes in each reach by an average of 27% (median = 19%), and in summer by an average of 30% (median = 26%). The results of the sensitivity analysis show that the absence of canopy cover increases the maximum watershed-wide riverine DOC elimination via photomineralization along the 611 km flow path almost 3-fold in each flow scenario (Table S4), and the mean absolute fluxes increased 3- to 4-fold. In summer, 1st order streams have the highest canopy shading, with an average of 35% reduction in absolute fluxes per reach, while in higher stream orders and in winter there is not a clear trend in shading based on stream order. Without canopy cover in summer median flows, the mean photomineralization flux in first order streams is 40.0 mg-C m^{-2} day^{-1}; this mean drops to 13.7 mg-C m^{-2} day^{-1} when canopy cover is included. This finding lends support to existing research showing that lakes or coastal river plumes with low total shading due to their width and shape can significantly reduce fluxes via photomineralization. In our study, the dramatic increase in mean reach photomineralization fluxes when canopy cover is excluded indicates

that forested watersheds, including temperate but also potentially tropical and boreal forests, are highly impacted by canopy cover and that this driver must be included when considering riverine photochemistry.

The sensitivity scenario that tests the impact of having infinite depth in all stream orders additionally supports the work that has shown that deeper lentic water bodies can have greater relative photochemical DOC loss. In Q_{98} flows, 41.2% of the DOC parcel traveling the 611 km flow path could be photomineralized if there were an infinite stream depth. While it is completely unrealistic that an entire watershed has depths that allow for all incoming solar irradiation to be absorbed, these high relative losses show that river depths significantly limit photomineralization capacity. In the other extreme sensitivity analysis scenario, which tests the absence of any light attenuation ($K_d = 0$), watershed-scale riverine DOC elimination along the 611 km flow path reaches 31.2% at Q_2 flows. However, given that we neglect the impact of TSS on $K_{d,\lambda}$, it is more likely that our overall photomineralization fluxes are overestimated, particularly at high flows where TSS is larger.

3.3. Other Considerations

It is worth reiterating that our model focuses solely on the impact of photomineralization on fluxes and concentrations of DOC within the riverine portions of the watershed, and does not consider the role of photobleaching on DOC chemistry and function. Thus, we do not rule out the potential for photo-alteration to play a meaningful role in terms of governing overall DOC chemistry, fate and impact along the entire river continuum when lentic and estuarine water bodies are included, or in the production of other important constituents during photooxidation. Given that the existing work has shown a single lake can eliminate more than 10% of the DOC (i.e., $R_r > 0.10$), and that approximately one quarter of the reaches in the CRW are classified as lentic, it is probable that the cumulative watershed elimination could be important when lentic systems are included. Previous studies have additionally shown for both rivers and estuaries that photobleaching or photo-bleachable DOC represents a major portion (>50%) of the DOC pool, despite possibly minor DOC photomineralization (Clark et al, 2020; Fichot & Benner, 2014; Yoon et al., 2021). We further note that our study does not directly compare photomineralization rates with bio-mineralization (respiration) rates, which has been a metric used in past studies to identify photo-alteration as an important (Cory et al., 2014) or unimportant process (Rocher-Ros et al, 2021). We can make some broad conclusions by comparing our very low uptake velocities for photomineralization (mean = 0.0054 m day^{-1}) with those for bio-mineralization or bulk DOC processing in other New England rivers (e.g., Wollheim et al. (2015) who found average uptake velocities at least an order of magnitude larger than ours, ~0.039 m day^{-1}), which suggest that photomineralization represents a negligible portion of the bulk DOC processing, except in outlier conditions. Our model sensitivity analysis shows considerable increases in photomineralization fluxes in the absence of canopy cover. This further supports the notion that photomineralization may be minor compared with bio-mineralization, due to the significant impacts that canopy has on reducing incoming solar irradiation (Supplementary Material Section S2).

4. Conclusions

We have developed the first model that quantifies photomineralization across all river reaches across a gradient of flows and seasons for the lotic sections of a large temperate watershed, taking into consideration both reaction and transport rates. We examined uptake velocities, reach-specific relative photomineralization rates, and whole-watershed riverine photomineralization rates using a variety of model assumptions and scenarios. The absolute areal photomineralization rates we calculate are within observed ranges for freshwaters, and are controlled by a combination of stream depth and DOC concentration, which we use to identify the thresholds separating four conditions for photomineralization: (i) maximum uptake velocity flux per DOC concentration (ii$_a$) substrate (DOC) limited (ii$_b$) depth-limited, and (iii) substrate (DOC) and depth excess. We show that even for high absolute photomineralization fluxes, uptake velocities are typically at least an order of magnitude smaller than other reported instream processes such as biomineralization or denitrification. Our results further indicate that due to the high flows and associated low water residence times in rivers, lotic photomineralization fluxes are limited by short transport timescales. As a result, relative to daily DOC fluxes through river reaches of all stream orders, photomineralization is a negligible DOC consumption process. We show that relative DOC elimination via photomineralization is highest during

summer drought conditions (i.e., very low flows), and in lower stream orders. During summer drought conditions, at most, a parcel of DOC following the longest flow path of 611 km through the riverine portions of the Connecticut River Watershed will lose 12.4% of its mass via complete photomineralization to DIC, but the average flow path length is less than half this distance in the CRW from headwaters to outlet. In median flows and mean light intensities, for an average watershed travel distance, 3%–5% of the DOC fluxes are eliminated. Keeping in mind that our results exclude the impacts of ice and cloud cover, and water column attenuation by TSS, "true" photomineralization rates are likely much lower. Lastly, we show that failing to account for canopy cover shading can result in up to a four-fold overestimation of photomineralization fluxes in temperate rivers. Thus, we conclude that photomineralization is not a significant, direct sink of DOC within the CRW.

Data Availability Statement

The hydrological model and results are available at https://zenodo.org/record/4135953#.YFqESOYpB24. The NHD Plus HR river network data is available at https://www.usgs.gov/core-science-systems/ngp/national-hydrography/access-national-hydrography-products. Connecticut River sampling site information, DOC concentration and discharge data are available in the supplementary material for the publication https://doi.org/10.1007/s10021-020-00514-7. Canopy cover photographs and associated data used to constrain the bagged tree regression models are available at https://doi.org/10.4231/0R47-4F65. The SMARTS2 model is available at https://solarconsultingservices.com/smarts.php.

References

Aarnos, H., Gélinas, Y., Kasurinen, V., Gu, Y., Puupponen, V. M., & Vähätalo, A. V. (2018). Photochemical mineralization of terrigenous DOC to dissolved inorganic carbon in ocean. *Global Biogeochemical Cycles*, *32*(2), 250–266. https://doi.org/10.1002/2017gb005698

Allesson, L., Koehler, B., Thrane, J. E., Andersen, T., & Hessen, D. O. (2020). *The role of photomineralization for CO_2 emissions in boreal lakes along a gradient of dissolved organic matter*. (1st ed., Vol. 66, pp. 158–170). Limnology and Oceanography.

Amon, R., & Benner, R. (1996). Photochemical and microbial consumption of dissolved organic carbon and dissolved oxygen in the Amazon River system. *Geochimica et Cosmochimica Acta*, *60*(10), 1783–1792. https://doi.org/10.1016/0016-7037(96)00055-5

Battin, T. J., Luyssaert, S., Kaplan, L. A., Aufdenkampe, A. K., Richter, A., & Tranvik, L. J. (2009). The boundless carbon cycle. *Nature Geoscience*, *2*(9), 598–600. https://doi.org/10.1038/ngeo618

Berggren, M., Klaus, M., Selvam, B. P., Ström, L., Laudon, H., Jansson, M., & Karlsson, J. (2018). Quality transformation of dissolved organic carbon during water transit through lakes: Contrasting controls by photochemical and biological processes. *Biogeosciences*, *15*(2), 457–470. https://doi.org/10.5194/bg-15-457-2018

Bertilsson, S., & Tranvik, L. J. (2000). Photochemical transformation of dissolved organic matter in lakes. *Limnology & Oceanography*, *45*(4), 753–762. https://doi.org/10.4319/lo.2000.45.4.0753

Bowen, J. C., Kaplan, L. A., & Cory, R. M. (2020a). Photodegradation disproportionately impacts biodegradation of semi-labile DOM in streams. *Limnology & Oceanography*, *65*(1), 13–26. https://doi.org/10.1002/lno.11244

Bowen, J. C., Ward, C., Kling, G., & Cory, R. (2020b). Arctic amplification of global warming strengthened by sunlight oxidation of permafrost carbon to CO_2. *Geophysical Research Letters*, *47*(12), e2020GL087085. https://doi.org/10.1029/2020gl087085

Brinkerhoff, C., Raymond, P., Maavara, T., Ishitsuka, Y., Aho, K., & Gleason, C. (2021). Lake morphometry and river network controls on evasion of terrestrially sourced headwater CO_2. *Geophysical Research Letters*, *48*(1), e2020GL090068. https://doi.org/10.1029/2020gl090068

Buiteveld, H., Hakvoort, J., & Donze, M. (1994) *Optical properties of pure water. Ocean optics XII* (pp. 174–183). International Society for Optics and Photonics.

Buto, S. G., & Anderson, R. D. (2020). *NHDPlus high resolution (NHDPlus HR)---A hydrography framework for the nation* (pp. 2327–6932). US Geological Survey.

Clark, J., Long, W., & Hood, R. (2020). A comprehensive estuarine dissolved organic carbon budget using an enhanced biogeochemical model. *Journal of Geophysical Research: Biogeosciences*, *125*(5), e2019JG005442. https://doi.org/10.1029/2019jg005442

Cole, J. J., Prairie, Y. T., Caraco, N. F., McDowell, W. H., Tranvik, L. J., Striegl, R. G., et al. (2007). Plumbing the global carbon cycle: Integrating inland waters into the terrestrial carbon budget. *Ecosystems*, *10*(1), 172–185. https://doi.org/10.1007/s10021-006-9013-8

Cory, R. M., & Kling, G. W. (2018). Interactions between sunlight and microorganisms influence dissolved organic matter degradation along the aquatic continuum. *Limnology and Oceanography Letters*, *3*(3), 102–116. https://doi.org/10.1002/lol2.10060

Cory, R. M., Ward, C. P., Crump, B. C., & Kling, G. W. (2014). Sunlight controls water column processing of carbon in arctic fresh waters. *Science*, *345*(6199), 925–928. https://doi.org/10.1126/science.1253119

Creech, E., Hosen, J. D., & Raymond, P. (2021). *Connecticut River watershed riparian canopy data*. https://purr.purdue.edu/publications/3732/1

Creed, I. F., McKnight, D. M., Pellerin, B. A., Green, M. B., Bergamaschi, B. A., Aiken, G. R., et al. (2015). The river as a chemostat: Fresh perspectives on dissolved organic matter flowing down the river continuum. *Canadian Journal of Fisheries and Aquatic Sciences*, *72*(8), 1272–1285. https://doi.org/10.1139/cjfas-2014-0400

Davies-Colley, R. J., & Nagels, J. W. (2008). Predicting light penetration into river waters. *Journal of Geophysical Research*, *113*(G3).

Detenbeck, N. E., Morrison, A. C., Abele, R. W., & Kopp, D. A. (2016). Spatial statistical network models for stream and river temperature in New England, USA. *Water Resources Research*, *52*(8), 6018–6040. https://doi.org/10.1002/2015wr018349

Dittmar, T., & Stubbins, A. (2014). *Dissolved organic matter in aquatic systems. Treatise on geochemistry* (2nd ed., pp. 125–156). Elsevier. https://doi.org/10.1016/b978-0-08-095975-7.01010-x

Doyle, M. W., Stanley, E. H., Strayer, D. L., Jacobson, R. B., & Schmidt, J. C. (2005). Effective discharge analysis of ecological processes in streams. *Water Resources Research*, *41*(11). https://doi.org/10.1029/2005wr004222

Ensign, S. H., & Doyle, M. W. (2006). Nutrient spiraling in streams and river networks. *Journal of Geophysical Research*, *111*(G4). https://doi.org/10.1029/2005jg000114

Fichot, C. G., & Benner, R. (2014). The fate of terrigenous dissolved organic carbon in a river-influenced ocean margin. *Global Biogeochemical Cycles*, *28*(3), 300–318. https://doi.org/10.1002/2013gb004670

Gao, H., & Zepp, R. G. (1998). Factors influencing photoreactions of dissolved organic matter in a coastal river of the southeastern United States. *Environmental Science & Technology*, *32*(19), 2940–2946. https://doi.org/10.1021/es9803660

Gareis, J. A., Lesack, L. F., & Bothwell, M. L. (2010). Attenuation of in situ UV radiation in Mackenzie Delta lakes with varying dissolved organic matter compositions. *Water Resources Research*, *46*(9). https://doi.org/10.1029/2009wr008747

Granéli, W., Lindell, M., & Tranvik, L. (1996). Photo-oxidative production of dissolved inorganic carbon in lakes of different humic content. *Limnology & Oceanography*, *41*(4), 698–706. https://doi.org/10.4319/lo.1996.41.4.0698

Gueymard, C. (1995). *SMARTS2: A simple model of the atmospheric radiative transfer of sunshine: Algorithms and performance assessment*. Florida Solar Energy Center Cocoa.

Gueymard, C. A. (2019). The SMARTS spectral irradiance model after 25 years: New developments and validation of reference spectra. *Solar Energy*, *187*, 233–253. https://doi.org/10.1016/j.solener.2019.05.048

Hansen, A. M., Kraus, T. E., Pellerin, B. A., Fleck, J. A., Downing, B. D., & Bergamaschi, B. A. (2016). Optical properties of dissolved organic matter (DOM): Effects of biological and photolytic degradation. *Limnology & Oceanography*, *61*(3), 1015–1032. https://doi.org/10.1002/lno.10270

Helms, J. R., Glinski, D. A., Mead, R. N., Southwell, M. W., Avery, G. B., Kieber, R. J., & Skrabal, S. A. (2014). Photochemical dissolution of organic matter from resuspended sediments: Impact of source and diagenetic state on photorelease. *Organic Geochemistry*, *73*, 83–89. https://doi.org/10.1016/j.orggeochem.2014.05.011

Hirsch, R. M., Moyer, D. L., & Archfield, S. A. (2010). Weighted regressions on time, discharge, and season (WRTDS), with an application to Chesapeake Bay river inputs. *JAWRA Journal of the American Water Resources Association*, *46*(5), 857–880. https://doi.org/10.1111/j.1752-1688.2010.00482.x

Hosen, J., Aho, K., Fair, J., Kyzivat, E., Matt, S., Morrison, J., et al. (2021). Source switching maintains dissolved organic matter chemostasis across discharge levels in a large temperate river network. *Ecosystems*, *24*, 227–247.

Julian, J., Doyle, M., & Stanley, E. (2008). Empirical modeling of light availability in rivers. *Journal of Geophysical Research: Biogeosciences*, *113*(G3). https://doi.org/10.1029/2007jg000601

Kaplan, L., & Cory, R. (2016). *Dissolved organic matter in stream ecosystems: Forms, functions, and fluxes of watershed tea, Stream ecosystems in a changing environment* (pp. 241–320). Elsevier. https://doi.org/10.1016/b978-0-12-405890-3.00006-3

Kirk, J. T. (1994). *Light and photosynthesis in aquatic ecosystems*. Cambridge University Press.

Koehler, B., Broman, E., & Tranvik, L. J. (2016). Apparent quantum yield of photochemical dissolved organic carbon mineralization in lakes. *Limnology & Oceanography*, *61*(6), 2207–2221. https://doi.org/10.1002/lno.10366

Koehler, B., Landelius, T., Weyhenmeyer, G. A., Machida, N., & Tranvik, L. J. (2014). Sunlight-induced carbon dioxide emissions from inland waters. *Global Biogeochemical Cycles*, *28*(7), 696–711. https://doi.org/10.1002/2014gb004850

Krogh, A. (1934). Conditions of life in the ocean. *Ecological Monographs*, *4*(4), 422–429. https://doi.org/10.2307/1961648

Logozzo, L., Tzortziou, M., Neale, P., & Clark, B. (2021). Photochemical and microbial degradation of chromophoric dissolved organic matter exported from tidal marshes. *Journal of Geophysical Research: Biogeosciences*, *126*(4), e2020JG005744. https://doi.org/10.1029/2020jg005744

Maavara, T., Chen, Q., Van Meter, K., Brown, L. E., Zhang, J., Ni, J., & Zarfl, C. (2020). River dam impacts on biogeochemical cycling. *Nature Reviews Earth & Environment*, *1*, 103–116. https://doi.org/10.1038/s43017-019-0019-0

Macdonald, M. J., & Minor, E. C. (2013). Photochemical degradation of dissolved organic matter from streams in the western Lake Superior watershed. *Aquatic Sciences*, *75*(4), 509–522. https://doi.org/10.1007/s00027-013-0296-5

Mann, P., Davydova, A., Zimov, N., Spencer, R., Davydov, S., Bulygina, E., et al. (2012). Controls on the composition and lability of dissolved organic matter in Siberia's Kolyma River basin. *Journal of Geophysical Research*, *117*(G1). https://doi.org/10.1029/2011jg001798

Miller, W. L., & Zepp, R. G. (1995). Photochemical production of dissolved inorganic carbon from terrestrial organic matter: Significance to the oceanic organic carbon cycle. *Geophysical Research Letters*, *22*(4), 417–420. https://doi.org/10.1029/94gl03344

Mineau, M. M., Wollheim, W. M., Buffam, I., Findlay, S. E., Hall, R. O., Jr, Hotchkiss, E. R., et al. (2016). Dissolved organic carbon uptake in streams: A review and assessment of reach-scale measurements. *Journal of Geophysical Research: Biogeosciences*, *121*(8), 2019–2029. https://doi.org/10.1002/2015jg003204

Moore, R. B., McKay, L. D., Rea, A. H., Bondelid, T. R., Price, C. V., Dewald, T. G., & Johnston, C. M. (2019). *User's guide for the national hydrography dataset plus (NHDPlus) high resolution* (pp. 2331–1258). US Geological Survey.

Mopper, K., Kieber, D. J., & Stubbins, A. (2015). Marine photochemistry of organic matter: Processes and impacts. *Biogeochemistry of marine dissolved organic matter*. 389–450. https://doi.org/10.1016/b978-0-12-405940-5.00008-x

Mulholland, P. J., Helton, A. M., Poole, G. C., Hall, R. O., Hamilton, S. K., Peterson, B. J., et al. (2008). Stream denitrification across biomes and its response to anthropogenic nitrate loading. *Nature*, *452*(7184), 202–205. https://doi.org/10.1038/nature06686

Niu, X.-Z., Harir, M., Schmitt-Kopplin, P., & Croué, J.-P. (2019). Sunlight-induced phototransformation of transphilic and hydrophobic fractions of Suwannee River dissolved organic matter. *The Science of the Total Environment*. *694*, 133737. https://doi.org/10.1016/j.scitotenv.2019.133737

Novo, E. M. L. M., Steffen, C. A., & Braga, C. Z. F. (1991). Results of a laboratory experiment relating spectral reflectance to total suspended solids. *Remote Sensing of Environment*, *36*(1), 67–72. https://doi.org/10.1016/0034-4257(91)90031-z

Opsahl, S., & Benner, R. (1998). Photochemical reactivity of dissolved lignin in river and ocean waters. *Limnology & Oceanography*, *43*(6), 1297–1304. https://doi.org/10.4319/lo.1998.43.6.1297

Osburn, C. L., Retamal, L., & Vincent, W. F. (2009). Photoreactivity of chromophoric dissolved organic matter transported by the Mackenzie River to the Beaufort Sea. *Marine Chemistry*, *115*(1–2), 10–20. https://doi.org/10.1016/j.marchem.2009.05.003

Phlips, E., Aldridge, F., Schelske, C., & Crisman, T. L. (1995). Relationships between light availability, chlorophyll a, and tripton in a large, shallow subtropical lake. *Limnology & Oceanography*, *40*(2), 416–421. https://doi.org/10.4319/lo.1995.40.2.0416

Raymond, P. A., Hartmann, J., Lauerwald, R., Sobek, S., McDonald, C., Hoover, M., et al. (2013). Global carbon dioxide emissions from inland waters. *Nature*, *503*(7476), 355–359. https://doi.org/10.1038/nature12760

Raymond, P. A., Saiers, J. E., & Sobczak, W. V. (2016). Hydrological and biogeochemical controls on watershed dissolved organic matter transport: Pulse-shunt concept. *Ecology*, *97*(1), 5–16. https://doi.org/10.1890/14-1684.1

Raymond, P. A., & Spencer, R. G. (2015). *Riverine DOM, Biogeochemistry of marine dissolved organic matter* (pp. 509–533). Elsevier. https://doi.org/10.1016/b978-0-12-405940-5.00011-x

Rocher-Ros, G., Harms, T. K., Sponseller, R. A., Väisänen, M., Mörth, C. M., & Giesler, R. (2021). Metabolism overrides photo-oxidation in CO_2 dynamics of Arctic permafrost streams. *Limnology and Oceanography*, *66*(S1), S169–S181.

Rose, L. A., Karwan, D. L., & Godsey, S. E. (2018). Concentration–discharge relationships describe solute and sediment mobilization, reaction, and transport at event and longer timescales. *Hydrological Processes*, *32*(18), 2829–2844. https://doi.org/10.1002/hyp.13235

Schlesinger, W. H., & Melack, J. M. (1981). Transport of organic carbon in the world's rivers. *Tellus*, *33*(2), 172–187. https://doi.org/10.3402/tellusa.v33i2.10706

Selvam, B. P., Lapierre, J.-F., Soares, A. R., Bastviken, D., Karlsson, J., & Berggren, M. (2019). Photo-reactivity of dissolved organic carbon in the freshwater continuum. *Aquatic Sciences*, *81*(4), 57. https://doi.org/10.1007/s00027-019-0653-0

Shiller, A. M., Duan, S., van Erp, P., & Bianchi, T. S. (2006). Photo-oxidation of dissolved organic matter in river water and its effect on trace element speciation. *Limnology & Oceanography*, *51*(4), 1716–1728. https://doi.org/10.4319/lo.2006.51.4.1716

Spencer, R. G., Aiken, G. R., Dornblaser, M. M., Butler, K. D., Holmes, R. M., Fiske, G., et al. (2013). Chromophoric dissolved organic matter export from US rivers. *Geophysical Research Letters*, *40*(8), 1575–1579. https://doi.org/10.1002/grl.50357

Stream Solute Workshop, (1990). Concepts and methods for assessing solute dynamics in stream ecosystems. *Journal of the North American Benthological Society*, *9*(2), 95–119. https://doi.org/10.2307/1467445

Stubbins, A., Law, C., Uher, G., & Upstill-Goddard, R. (2011). Carbon monoxide apparent quantum yields and photoproduction in the Tyne estuary. *Biogeosciences*, *8*(3), 703–713. https://doi.org/10.5194/bg-8-703-2011

Stubbins, A., Spencer, R. G., Chen, H., Hatcher, P. G., Mopper, K., Hernes, P. J., et al. (2010). Illuminated darkness: Molecular signatures of Congo River dissolved organic matter and its photochemical alteration as revealed by ultrahigh precision mass spectrometry. *Limnology & Oceanography*, *55*(4), 1467–1477. https://doi.org/10.4319/lo.2010.55.4.1467

Stubbins, A., Uher, G., Law, C. S., Mopper, K., Robinson, C., & Upstill-Goddard, R. C. (2006). Open-ocean carbon monoxide photoproduction. *Deep Sea Research Part II*, *53*(14–16), 1695–1705. https://doi.org/10.1016/j.dsr2.2006.05.011

USGS. (2020). *National water information system.* https://waterdata.usgs.gov/nwis/rt%252020

Vähätalo, A. V., Salkinoja-Salonen, M., Taalas, P., & Salonen, K. (2000). Spectrum of the quantum yield for photochemical mineralization of dissolved organic carbon in a Humic lake. *Limnology & Oceanography*, *45*(3), 664–676. https://doi.org/10.4319/lo.2000.45.3.0664

V.-Balogh, K., Németh, B., & Vörös, L. (2009). Specific attenuation coefficients of optically active substances and their contribution to the underwater ultraviolet and visible light climate in shallow lakes and ponds. *Hydrobiologia*, *632*(1), 91–105. https://doi.org/10.1007/s10750-009-9830-9

Vodacek, A., Blough, N. V., DeGrandpre, M. D., DeGrandpre, M. D., & Nelson, R. K. (1997). Seasonal variation of CDOM and DOC in the Middle Atlantic Bight: Terrestrial inputs and photooxidation. *Limnology & Oceanography*, *42*(4), 674–686. https://doi.org/10.4319/lo.1997.42.4.0674

Vollenweider, R. A. (1975). Input-output models. *Schweizerische Zeitschrift für Hydrologie*, *37*(1), 53–84. https://doi.org/10.1007/bf02505178

White, E. M., Kieber, D. J., Sherrard, J., Miller, W. L., & Mopper, K. (2010). Carbon dioxide and carbon monoxide photoproduction quantum yields in the Delaware Estuary. *Marine Chemistry*, *118*(1–2), 11–21. https://doi.org/10.1016/j.marchem.2009.10.001

Wollheim, W. M., Bernal, S., Burns, D. A., Czuba, J., Driscoll, C. T., Hansen, A., et al. (2018). River network saturation concept: Factors influencing the balance of biogeochemical supply and demand of river networks. *Biogeochemistry*, *141*(3), 503–521. https://doi.org/10.1007/s10533-018-0488-0

Wollheim, W. M., Stewart, R. J., Aiken, G. R., Butler, K. D., Morse, N. B., & Salisbury, J. (2015). Removal of terrestrial DOC in aquatic ecosystems of a temperate river network. *Geophysical Research Letters*, *42*(16), 6671–6679. https://doi.org/10.1002/2015gl064647

Xie, H., Zafiriou, O. C., Cai, W.-J., Zepp, R. G., & Wang, Y. (2004). Photooxidation and its effects on the carboxyl content of dissolved organic matter in two coastal rivers in the southeastern United States. *Environmental Science & Technology*, *38*(15), 4113–4119. https://doi.org/10.1021/es035407t

Yoon, B., Hosen, J. D., Kyzivat, E. D., Fair, J. H., Weber, L. C., Aho, K. S., et al. (2021). Export of photolabile and photoprimable dissolved organic carbon from the Connecticut River. *Aquatic Sciences*, *83*(2), 1–17. https://doi.org/10.1007/s00027-021-00778-8

Ziegler, S., & Benner, R. (2000). Effects of solar radiation on dissolved organic matter cycling in a subtropical seagrass meadow. *Limnology & Oceanography*, *45*(2), 257–266. https://doi.org/10.4319/lo.2000.45.2.0257

Reference From the Supporting Information

Hosen, J. D., Aho, K. S., Appling, A. P., Creech, E. C., Fair, J. H., Hail, R. O., et al. (2019). Enhancement of primary production during drought in a temperate watershed is greater in larger rivers than headwater streams. *Limnology and Oceanography*. *64*(4), 1458–1472.